

37 Non-linear non-parametric geostatistical rock-physics inversion of
38 elastic attributes for petrophysical properties using direct
39 multivariate simulation

40 Leandro Passos de Figueiredo^a, Dario Grana^b, Bruno B. Rodrigues^c and Alexandre Emerick^c

41 ^a LTrace Geosciences

42 ^bDepartment of Geology and Geophysics, University of Wyoming

43 ^cPetrobras, Rio de Janeiro, Brazil

44

45 ARTICLE INFO

46 **Keywords:**

47 Rock-physics inversion
48 Petrophysical properties
49 non-parametric distributions
50 Geostatistical simulations
51 Time-lapse inversion

52

53

54

55

56

57

58

59

60

61

62

63

64

65

66

67 CRediT authorship contribution statement

68 **Leandro Passos de Figueiredo:** Theory, Coding, application, writing . **Dario Grana:** Theory, application,
69 reviewing. **Bruno B. Rodrigues:** Application, reviewing. **Alexandre Emerick:** Project managing, application, re-
70 viewing.

71 **1. Introduction**

72 Seismic and rock-physics inversion methods are critical steps of seismic reservoir characterization process, since
73 they allow estimating the petrophysical properties of saturated porous rocks based on geophysical data (Avseth et al.,
74 2005; Doyen, 2007; Grana et al., 2021). Many applications focus on estimating porosity, water saturation, and min-
75 eralogy in clastic reservoirs (Bosch et al., 2009; Grana, 2016; Fjeldstad and Grana, 2017; Aleardi et al., 2017), but
76 rock physics formulations have also been extended in to carbonates for the prediction of the pore shape, aspect ratio,
77 and fracture geometry (Teillet et al., 2021; Guo et al., 2022, 2023). The estimation of petrophysical properties from
78 measured data is generally formulated as an inverse problem.

ORCID(s): 0000-0000-0000-0000 (L.P.d. Figueiredo)

79 Geophysical inverse problems are typically ill-posed due to approximations of the physical models and observational errors in the measurements (Tarantola, 2005; Sen, 2006). For this reason, the solution of the geophysical inverse
 80 problem is often non unique. Hence, probabilistic approaches are generally preferred to deterministic methods due to
 81 their ability to quantify the uncertainty in the solution (Bosch et al., 2010; Grana et al., 2022a). These methods provide
 82 a framework for quantifying uncertainties by assessing the probability distributions of model variables.
 83

84 The proposed methods for seismic and rock-physics inversion can be classified as two-step or single-step approaches
 85 (Grana et al., 2022a). The two-step approach involves using seismic data first to estimate elastic properties via seismic
 86 inversion and then inverting such properties to estimate the petrophysical properties (Bachrach, 2006; Grana and
 87 Della Rossa, 2010; Shahraeeni and Curtis, 2011; Grana, 2016; Aleardi, 2018; Grana et al., 2022b). Instead, the single-
 88 step approach integrates seismic and rock-physics modeling into a single inverse problem, directly converting seismic
 89 data into petrophysical properties (Fjeldstad and Grana, 2017; Aleardi et al., 2017; Liu and Grana, 2018; de Figueiredo
 90 et al., 2018, 2019). The two-step approach is the most common due to its simplicity, the feasible computational time,
 91 and the robustness of linearized seismic inversion methods (Buland and Omre, 2003). In this work, we focus on the
 92 rock-physics component of the inversion for the estimation of petrophysical properties from elastic attributes, which
 93 we refer to as rock-physics inversion (Grana et al., 2022a). The main challenge of the rock-physics inversion is the non
 94 linearity of the rock physics model and the non-Gaussianity of the multivariate distribution of petrophysical properties.
 95

96 Deterministic and probabilistic methods have been proposed for rock-physics inversion (Bosch et al., 2010; Grana
 97 et al., 2022a). Probabilistic approaches are often based on geostatistical simulation techniques to obtain an ensemble
 98 of spatially correlated realizations of petrophysical properties conditioned on elastic properties (Doyen, 2007;
 99 Leonardo Azevedo, 2017; de Figueiredo et al., 2018; Grana et al., 2024). The multiple model realizations generated
 100 with this approach are used for uncertainty quantification, sensitivity analysis, and to better inform decision-making
 101 processes in reservoir engineering (Caers, 2011). Many geostatistical approaches are based on the Gaussian sequential
 102 simulation (SGS) algorithm (Doyen, 2007; Grana et al., 2021), which presents limitations for reproducing complex
 103 non-parametric multivariate distributions with non linear and heteroscedastic relations among the variables. Such
 104 relations are often found in real data in reservoir modeling.

105 As an alternative to SGS, the Direct Sequential simulation (DSS) algorithm proposed by Soares (2001) can be applied
 106 to non-parametric distributions, where the random values are drawn directly from the target distribution. Hence,
 107 DSS reproduces the marginal distribution of the variable without any additional transformation. The extension to multivariate
 108 problems is achieved using conditional distributions, as shown in Horta and Soares (2010). More recently,
 109 different approaches for geostatistical simulations of variables for complex non-parametric multivariate distributions
 110 have been proposed (Barnett et al., 2014; de Figueiredo et al., 2021; Avalos and Ortiz, 2023b; Abulkhair et al., 2023;
 111 Avalos and Ortiz, 2023a). Among these methods, the Direct Multivariate Simulation (DMS) algorithm, proposed in

(de Figueiredo et al., 2021), is an efficient method based on stepwise conditional transformations. This algorithm uses empirical cumulative distributions to perform simulations at low computational cost (de Figueiredo et al., 2021). The stepwise conditional transformation consists of a generalization of the normal score and back transformation for multivariate distributions. This method enables transforming multiple independent realizations of Gaussian random fields into realizations of non-parametric multivariate random fields. In other words, DMS allows generating realizations of a statistical model where multiple random variables are spatially or temporally related across a domain, without making assumptions about the specific underlying probability distribution of the data.

In this work, we adopt the DMS approach to generate multiple geostatistical realizations conditioned on elastic properties for rock-physics inversion. The inversion approach is based on Monte Carlo sampling to generate a training dataset using a non-linear rock-physics model and non-parametric multivariate distribution. The DMS-based inversion efficiently computes the conditional distribution and generates spatially correlated geostatistical realizations. The methodology is validated through two applications. The first example is based on real well log data, whereas the second application is a synthetic time-lapse seismic dataset. In the first example, we estimate multiple realizations of petrophysical volumetric fractions conditioned on elastic properties based on a 6-variate joint distribution. In the second example, we estimate multiple realizations of porosity and fluid changes from changes in elastic properties based on a 7-variate joint distribution. In both applications, we demonstrate that the proposed algorithm is extremely efficient compared to a traditional implementation based on the calculation of conditional distributions from the joint distribution (Grana and Della Rossa, 2010; Grana et al., 2021). Furthermore, the multiple realizations strictly follow the non-parametric joint distributions, with non-linear and heteroscedastic relations among variables.

2. Methods

The proposed method is a geostatistical approach for rock-physics inversion based on a statistical rock physics model and the DMS algorithm. We first describe the statistical approach to rock-physics modeling, then we introduce the DMS algorithm for efficiently generating geostatistical realizations, and we finally discuss the application of the method to rock-physics inversion and time-lapse rock-physics inversion. For clarity, Table 1 shows the list of symbols used in this section.

Symbol	Description
\mathbf{m}	Elastic properties
\mathbf{r}	Petrophysical properties
e_m	Data and model error
Σ_m	Error covariance matrix
N_s	Number of Monte Carlo Samples (training data)
z	Arbitrary random variable
n	Total number of variables
p	Number of unknown variables
q	Number of measured variables
\mathbf{z}	Arbitrary random vector
\mathbf{x}_i	Spatial location
N	Number of grid points
$\mathbf{z}(\mathbf{x}_i)$	Random vector at position \mathbf{x}_i
Φ	Gaussian cumulative distribution
g	Gaussian distributed simulation
π	Facies
F	Number of facies
ϕ	Porosity
s_w	Water saturation
v_c	Volume of clay
V_p	P-wave velocity
V_s	S-wave velocity
ρ	Density
I_p	P-impedance

Table 1

Table of symbols.

136 2.1. Statistical rock-physics model

137 A rock-physics model is a set of theoretical equations used to compute elastic properties from petrophysical prop-
 138 erties (Mavko et al., 2009; Grana et al., 2021). In hydrocarbon reservoirs, the typical rock-physics model computes P- and
 139 S-wave velocities, and density, from porosity, fluid saturation, and mineral volumes. In statistical rock-physics mod-
 140 eling, the properties of interest are considered as random variables, and they are related to the random measurements
 141 through the rock-physics equations.

142 We assume that elastic and petrophysical properties are defined at each point of a discretized grid of N points, such
 143 as the seismic grid or a regular geocellular reservoir grid. Then, elastic properties are denoted as $\mathbf{m} \in \mathbb{R}^N$ and they
 144 are computed using a rock physics model as:

$$145 \mathbf{m} = \mathbf{f}(\mathbf{r}) + e_m, \quad (1)$$

146 where $\mathbf{r} \in \mathbb{R}^N$ represents the petrophysical properties, $\mathbf{f}(.)$ is the rock-physics model and e_m represents the error term
 147 that is assumed to be Gaussian with zero mean and covariance Σ_m (Grana and Della Rossa, 2010).

Because the rock-physics model is usually a non-bijective function and due to model and data errors, the solution

of the rock-physics inverse problem for the estimation of petrophysical properties is not unique (Grana et al., 2021). This problem can be numerically solved by computing the conditional distribution of the petrophysical properties, conditioned on the observed elastic properties from the joint probability density function (PDF) of both petrophysical and elastic properties as

$$p(\mathbf{r}|\mathbf{m}) = \frac{p(\mathbf{m}, \mathbf{r})}{p(\mathbf{m})}, \quad (2)$$

where the joint distribution $p(\mathbf{m}, \mathbf{r})$ is assumed to be non-parametric (Grana and Della Rossa, 2010).

The joint distribution $p(\mathbf{m}, \mathbf{r})$ is estimated based on a training dataset, such as a set of well logs representative of all possible reservoir conditions, or a set of Monte Carlo samples generated a statistical rock-physics model (Bachrach, 2006; Grana and Della Rossa, 2010). The joint distribution $p(\mathbf{m}, \mathbf{r})$ can be written as

$$p(\mathbf{m}, \mathbf{r}) = p(\mathbf{m}|\mathbf{r})p(\mathbf{r}), \quad (3)$$

where $p(\mathbf{r})$ is the prior distribution of the petrophysical properties, and $p(\mathbf{m}|\mathbf{r})$ is the conditional distribution (also called the likelihood function) of the elastic properties given the petrophysical ones.

Based on Equation 1 and on the Gaussian assumption for the error term e_m , the likelihood function $p(\mathbf{m}|\mathbf{r})$ is then written as a Gaussian distribution $\mathcal{N}(\mathbf{m}|\mathbf{f}(\mathbf{r}); \Sigma_m)$, where the mean is computed using the rock physics model and the covariance matrix is the covariance of the error:

$$p(\mathbf{m}, \mathbf{r}) \propto \mathcal{N}(\mathbf{m}|\mathbf{f}(\mathbf{r}); \Sigma_m)p(\mathbf{r}). \quad (4)$$

The joint distribution often presents multimodality due to the presence of multiple facies or rock types. We then assume that the prior distribution is a mixture model of F components, $p(\mathbf{r}) = \sum_{f=1}^F p(\mathbf{r}|\pi_f)p(\pi_f)$, where π is a categorical variable representing the facies and F is the number of facies. In this mixture model, each mode of the model is associated with a different facies. Then, we write the joint distribution as mixture model:

$$p(\mathbf{m}, \mathbf{r}) \propto \sum_{f=1}^F \mathcal{N}(\mathbf{m}|\mathbf{f}(\mathbf{r}); \Sigma_m)p(\mathbf{r}|\pi_f)p(\pi_f). \quad (5)$$

The prior distributions $p(\mathbf{r}|\pi_f)$ and $p(\pi_f)$ are generally defined based on core samples, well log data, and geological knowledge. The prior distribution should be large enough to account for all possible values of petrophysical and elastic properties.

Using Equation 5, we can adopt a Monte Carlo sampling to draw N_s samples of facies $\{\pi^i\}_{i=1,\dots,N_s}$ from the prior

¹⁶⁹ distribution $p(\pi)$, N_s samples of the petrophysical properties $\{\mathbf{r}^i\}_{i=1,\dots,N_s}$ from the distribution $p(\mathbf{r}|\pi^i)$, and N_s samples
¹⁷⁰ of the elastic properties $\{\mathbf{m}^i\}_{i=1,\dots,N_s}$ from the Gaussian distribution $\mathcal{N}(\mathbf{m}^i; \mathbf{f}(\mathbf{r}^i), \boldsymbol{\Sigma}_m)$. Due to the non-linearity of the
¹⁷¹ rock-physics model and the non-parametric assumption about the prior $p(\mathbf{r}|\pi)$, the joint distribution is a non-parametric
¹⁷² distribution and might present heteroscedasticity.

¹⁷³ **2.2. Direct multivariate simulation**

¹⁷⁴ DMS is a geostatistical method to generate multiple geostatistical realizations that strictly follow a non-parametric
¹⁷⁵ multivariate joint distribution with a large number of variables (de Figueiredo et al., 2021). The methodology is
¹⁷⁶ based on the stepwise conditional transformation, a generalization of the normal score and back transformation for
¹⁷⁷ multivariate distributions. The stepwise conditional transformation allows the transformation of multiple independent
¹⁷⁸ Gaussian geostatistical realizations into spatially correlated realizations of a non-parametric multivariate random field
¹⁷⁹ (Leuangthong and Deutsch, 2003).

¹⁸⁰ Given a set of n arbitrary random variables $z_j \in \mathbb{R}$ for $j = 1, \dots, n$ that follow a n -variate joint PDF $p(z_1, z_2, \dots, z_n)$,
¹⁸¹ the method performs a sequential sampling from the univariate distributions of the decomposition of the PDF, based
¹⁸² on the multiplication rule Gómez-Hernández and Journel (1993); Leuangthong and Deutsch (2003); Tarantola (2005);
¹⁸³ Bertsekas and Tsitsiklis (2008), i.e. the product of marginal and conditional PDFs:

$$p(z_1, z_2, \dots, z_n) = p(z_1)p(z_2|z_1)p(z_3|z_1, z_2)\dots p(z_n|z_1, \dots, z_{n-1}). \quad (6)$$

¹⁸⁴ The implementation of the methodology is summarized as follows:

- ¹⁸⁵ 1. Draw z_1 from the marginal distribution $p(z_1)$.
- ¹⁸⁶ 2. Draw z_2 from the conditional distribution $p(z_2|z_1)$ conditioned on the variable value drawn in the previous step.
- ¹⁸⁷ 3. Draw z_3 from the conditional distribution $p(z_3|z_1, z_2)$ conditioned on the variable values drawn in the previous
¹⁸⁸ steps.
- ¹⁸⁹ 4. Iteratively draw all the other variables z_j (for $j = 4, \dots, n$) from the conditional distribution $p(z_j|z_1, \dots, z_{j-1})$
¹⁹⁰ conditioned on the variable values drawn in the previous steps.

¹⁹¹ In practice, the stepwise sampling from univariate conditional distributions is performed by introducing a set of
¹⁹² auxiliary variables uniformly distributed $u_j \sim U(0, 1)$ and computing the desired variables z_j as

$$z_j = P^{-1}(u_j|z_1, \dots, z_{j-1}), \quad (7)$$

¹⁹³ where $P^{-1}(\cdot|z_1, \dots, z_{j-1})$ is the inverse cumulative distribution function of the PDF $p(z_j|z_1, \dots, z_{j-1})$ for $j = 2, \dots, n$.

194 The simulation process in DMS is highly efficient thanks to its implementation. The n-variate non-parametric PDF
 195 is directly estimated from the input training data. The conditioning process is performed by applying a threshold filter
 196 to select a subset of data of the conditioning variable. For example, for computing the distribution of the variable
 197 z_2 conditioned to the drawn value z_1^* , we select a subset of points from the training data that satisfies the following
 198 condition on z_1

$$z_1^* - \Delta z_1 \leq z_1 \leq z_1^* + \Delta z_1, \quad (8)$$

199 where Δz_1 is a threshold value of tolerance. In other words, the filtered subset is obtained by excluding from the
 200 training data all the points that are far from the conditioning value z_1^* .

201 Then, the cumulative distribution is directly estimated from the filtered subset by applying the empirical cumulative
 202 distribution technique. Using the same example of z^2 given z_1^* , to estimate the cumulative distribution $P(z_2|z_1^*)$, the
 203 empirical cumulative is given by

$$P(z_2|z_1^*) = \frac{h}{l} \quad (9)$$

204 where h is the number of elements lower than z_2 and l is the number of points of the filtered dataset. The number of
 205 elements h is obtained by simply sorting the samples of z_2 in increasing order.

206 If the variables are spatially correlated, we apply the Gaussian cumulative distribution $\Phi(.)$ to the Gaussian dis-
 207 tributed variable g , obtain a uniformly distributed variable u , and then we apply the non-parametric inverse cumulative
 208 P^{-1} to transform the variable into the target non-parametric distribution. We define the spatially correlated simulation
 209 $z_j \in \mathbb{R}^N$ in a discretized grid of N points, with grid points at locations $\{\mathbf{x}_i\}_{i=1,\dots,N}$. Then $z_j(\mathbf{x}_i)$ denotes the value of
 210 the variable z_j at location \mathbf{x}_i . We then sample spatially correlated simulations of $\{z_j\}_{j=1,\dots,n}$ from the non-parametric
 211 joint PDF using the following decomposition

$$z_j(\mathbf{x}_i) = P^{-1}(\Phi(g_j(\mathbf{x}_i))|z_1(\mathbf{x}_i), \dots, z_{j-1}(\mathbf{x}_i)), \quad (10)$$

212 where $P^{-1}(.|z_1(\mathbf{x}_i), \dots, z_{j-1}(\mathbf{x}_i))$ is the inverse cumulative distribution function of the PDF $p(z_j(\mathbf{x}_i)|z_1(\mathbf{x}_i), \dots, z_{j-1}(\mathbf{x}_i))$,
 213 $\Phi(.)$ is the Gaussian cumulative distribution function and $g_j(\mathbf{x}_i)$ is a stochastic realization of a Gaussian random field
 214 simulated by a traditional geostatistical method (de Figueiredo et al., 2021). The stochastic realization g_j of the Gaus-
 215 sian random field and the Gaussian cumulative distribution $\Phi(.)$ have zero mean and unit variance. The parameters of
 216 the variograms controlling the spatial correlation model are estimated from the well logs and geological knowledge.

217 Equation 10 enables the transformation of Gaussian distributed variables into the non-parametric target distribution

(Leuangthong and Deutsch, 2003; de Figueiredo et al., 2021). Conversely, the inverse transformation can be used to transform a set of non-parametric observations into a set of uncorrelated Gaussian distributed variables. For conditional realizations, this transformation is also applied to hard data (i.e. direct measurements of the unknown variables, such as well log data). Hence, to generate geostatistical realizations conditioned on hard data, we first transform direct measurements from the original domain into a Gaussian space, where conditional geostatistical realizations are simulated; then, non-parametric conditional simulations are obtained by transforming the conditional Gaussian realizations into the non-parametric space using Eq. 10.

The stepwise conditional transformation allows transferring the spatial correlations in the Gaussian simulations \mathbf{g}_j to the nonparametric realizations. When the transformation is highly non-linear, the spatial correlation might not be completely preserved in the non-parametric realizations. To overcome this limitation, we recommend to estimate the spatial correlation from the training dataset in the transformed Gaussian-distributed domain rather than in the original domain (de Figueiredo et al., 2021).

2.3. Geostatistical rock-physics inversion

The DMS method is then combined with statistical rock physics in a geostatistical rock-physics inversion for the prediction of petrophysical properties from elastic properties. In general, if the rock-physics inversion involves p petrophysical properties and q elastic attributes, the goal is to predict the conditional distribution $p(\mathbf{r}|\mathbf{m}) = p(r_1, \dots, r_p | m_1, \dots, m_q)$.

We present the geostatistical inversion method assuming $p = 3$ petrophysical properties and $q = 3$ elastic properties, but the inversion can be extended to any number of variables. The typical rock-physics inversion problem involves the estimation of porosity ϕ , water saturation s_w and clay volume v_c from P-wave velocity V_P , S-wave velocity V_S and density ρ . In this case, the solution of the rock-physics inverse problem is the conditional distribution $p(\mathbf{r}|\mathbf{m}) = p(\phi, s_w, v_c | V_P, V_S, \rho)$.

In the case of $p = 3$ and $q = 3$, the conditional distribution can be decomposed as

$$p(r_1, r_2, r_3 | m_1, m_2, m_3) = p(r_3 | m_1, m_2, m_3)p(r_2 | r_3, m_1, m_2, m_3)p(r_1 | r_2, r_3, m_1, m_2, m_3), \quad (11)$$

according to Eq. 6.

We assume that both petrophysical and elastic attributes are defined on the same grid of N points with grid points $\{\mathbf{x}_i\}_{i=1,\dots,N}$. Then, using the DMS approach, we sample multiple geostatistical realizations of the petrophysical properties $\mathbf{r}_1, \dots, \mathbf{r}_p$ conditioned on the elastic properties $\mathbf{m}_1, \dots, \mathbf{m}_q$. In practical applications conditioning elastic data $\mathbf{m}_1, \dots, \mathbf{m}_q$ are measured directly from well logs or are estimated from measured seismic data. If we assume three input variables in the elastic domain and three input variables in the petrophysical domain, the inversion methodology to sample non-parametric geostatistical realizations of petrophysical properties conditioned on the available elastic

247 attributes, is then summarized as follows:

- 248 1. Use a traditional geostatistical method to simulate three spatially correlated realizations $\{g_j(\mathbf{x}_i)\}$ for $j = r_1, r_2, r_3$
 249 and $i = 1, \dots, N$ of a Gaussian random field with zero mean and unit variance.
- 250 2. Compute a realization of r_1 with Eq. 10 conditioned on elastic properties:

$$r_1(\mathbf{x}_i) = P^{-1}(\Phi(g_{r_1}(\mathbf{x}_i)) | m_1(\mathbf{x}_i), m_2(\mathbf{x}_i), m_3(\mathbf{x}_i)) \quad (12)$$

- 251 3. Compute a realization of r_2 with Eq. 10 conditioned on elastic properties and $r_1(\mathbf{x}_i)$ obtained in the previous
 252 step:

$$r_2(\mathbf{x}_i) = P^{-1}(\Phi(g_{r_2}(\mathbf{x}_i)) | r_1(\mathbf{x}_i), m_1(\mathbf{x}_i), m_2(\mathbf{x}_i), m_3(\mathbf{x}_i)) \quad (13)$$

- 253 4. Compute a realization of r_3 with Eq. 10 conditioned on elastic properties, $r_1(\mathbf{x}_i)$, and $r_2(\mathbf{x}_i)$ obtained in the
 254 previous step:

$$r_3(\mathbf{x}_i) = P^{-1}(\Phi(g_{r_3}(\mathbf{x}_i)) | r_2(\mathbf{x}_i), r_1(\mathbf{x}_i), m_1(\mathbf{x}_i), m_2(\mathbf{x}_i), m_3(\mathbf{x}_i)). \quad (14)$$

- 255 In addition to the geostatistical realizations, we can also compute the median value by setting the cumulative distribu-
 256 tion equal to 0.5 in Eq. 10.

257 Furthermore, the geostatistical realizations and the median models can be conditioned on available hard data as
 258 discussed in de Figueiredo et al. (2021). To obtain hard data conditioning, we first apply the inverse of Eq. 10 to
 259 transform the hard data into the Gaussian distributed space; then, using a traditional Gaussian simulation method,
 260 we simulate three conditional realizations $\{g_j\}$ for $j = \phi, s_w, v_c$ of a Gaussian random field with zero mean and unit
 261 variance; finally, using the conditional realizations in steps 2-4, the data conditioning is achieved in the non-parametric
 262 realizations. For the median models, we apply a similar approach, but instead of using geostatistical realizations, we
 263 compute the realizations $\{g_j\}$ using simple kriging interpolation of the transformed measured data, assuming zero
 264 mean and unit variance.

265 The proposed algorithm is extremely efficient thanks to the DMS approach. A key aspect of the DMS implementa-
 266 tion is the application of the marginal and conditional distributions directly in the space $\{\mathbf{r}^i, \mathbf{m}^i\}_{i=1,\dots,N_s}$, which allows
 267 for the direct sampling of the joint distribution. The conditional distribution is obtained by applying filters to select
 268 the range of conditional values, whereas marginal distributions are computed directly from the statistics of the filtered

269 values (de Figueiredo et al., 2021). Moreover, DMS uses empirical cumulative distribution functions to obtain the
 270 target non-parametric distributions (van der Waerden et al., 1969; Berg and Harris, 2008).

271 The proposed method can be applied to any number p of petrophysical properties and any number of elastic at-
 272 tributes q . The method can also be extended to the time-dependent data, for example time-lapse seismic surveys with
 273 spatio-temporal dependent variables, for example spatially dependent porosity and spatio-temporal dependent fluid
 274 saturation. A schematic representation of the methodology is shown in Fig. 1.

275 3. Application

276 The methodology is validated through two applications. The first example uses real well log data to invert elas-
 277 tic properties (namely P- and S-wave velocities and density), for the prediction of petrophysical properties (namely
 278 porosity, clay volume, and water saturation). The second application employs a synthetic time-lapse model to invert
 279 time-lapse elastic properties (P-impedance and velocity ratio), to predict petrophysical properties (porosity and water
 280 saturation at different times). In these examples we demonstrate conditional simulations using elastic properties only
 281 as well as elastic properties and hard data.

282 3.1. Well log data application

283 This example is based on real well log data measured in a siliciclastic oil reservoir in the Norwegian Sea (Grana
 284 et al., 2021) to demonstrate the application of the method to an inverse problem for the estimation of petrophysical
 285 properties from elastic measurements. The available dataset is shown in Fig. 2 and it includes facies, P- and S-
 286 wave velocities, density, porosity, clay volume, and water saturation. The interval under study includes three different
 287 litho-fluid facies, namely shale, brine sand, and oil sand. The main sand reservoir layers are saturated by oil and are
 288 interbedded with thin shale layers in the upper part of the interval and brine-saturated sand layers in the lower part.

289 In this application, we use the proposed methodology to estimate the petrophysical properties of porosity, clay
 290 volume, and water saturation based on the elastic logs of P- and S-wave velocities and density. The predictions are
 291 validated using petrophysical logs. We first use Monte Carlo sampling to generate the training dataset from the joint
 292 distribution $p(\mathbf{m}, \mathbf{r})$ using Equation 5. Based on well log data, we assume a truncated Gaussian mixture model for the
 293 prior $p(\mathbf{r})$ and we assume that the mixture components $p(\mathbf{r}|\pi)$ are facies-dependent. Table 2 shows the parameters
 294 of the mixture distributions in each facies. The parameters are defined to fit the facies-dependent distributions to the
 295 experimental marginal histograms of the well logs in each facies. We draw 8000 samples from the shale facies, 3000
 296 from the brine sand facies and 4000 samples from the oil sand facies, where the number of samples per facies is defined
 297 according to their prior proportions.

298 Figs. 2d-f show the inverted median models (red) and 20 geostatistical realizations (gray) of porosity, clay volume

	shale	brine sand	oil sand
porosity	$\mathcal{N}(0.18, 0.036)$ [0, 0.4]	$\mathcal{N}(0.24, 0.017)$ [0, 0.4]	$\mathcal{N}(0.27, 0.018)$ [0, 0.4]
clay volume	$\mathcal{N}(0.3, 0.202)$ [0, 0.8]	$\mathcal{N}(0.07, 0.06)$ [0, 0.8]	$\mathcal{N}(0.09, 0.068)$ [0, 0.8]
water saturation	$\mathcal{N}(0.86, 0.211)$ [0, 1]	$\mathcal{N}(0.95, 0.02)$ [0, 1]	$\mathcal{N}(0.2, 0.347)$ [0, 1]

Table 2

Parameters of the prior Gaussian mixture model for porosity, clay volume and water saturation. $\mathcal{N}(\mu, \sigma)$ [min, max] denotes a truncated Gaussian distribution with mean μ and standard deviation σ , and truncated minimum and maximum values, min and max.

and saturation, respectively. The inverted median models of porosity and clay volume match the reference logs (black) very accurately, whereas the inverted median model of water saturation presents some mismatches in the lower part of the interval and a higher variability of the realizations, possibly due to the high bimodality of the reference distribution as well as the lower sensitivity of saturation to the elastic parameters. The set of multiple realizations show the uncertainty of the model, with large variability in water saturation.

The computational time depends on the number of samples, the number of properties, and the implementation parameters. At each point of the grid, the computational complexity of the prediction is $O(q \times N_s)$, and it scales linearly in the grid of the inversion, for all the N points of the grid. The main computational advantage of the implementation is the limited RAM usage of the DMS approach. We compare the RAM usage of the proposed DMS approach to the rock-physics inversion using non-parametric distributions proposed in Grana et al. (2021). The implementation in Grana et al. (2021) requires the storage of the multivariate joint distribution $p(\mathbf{m}, \mathbf{r})$. This distribution is computed once for the entire grid. However, because it has to be applied to all the N points of the grid, the distribution must be evaluated for all the possible combinations of the values of the variables \mathbf{m} and \mathbf{r} , and it must be stored in a matrix with dimensions $L^p \times L^q$, where p and q are the numbers of variables in \mathbf{m} and \mathbf{r} , and L is the size of the discretized domain of each property. This domain is defined by discretizing the interval between the minimum and maximum values of each variable in L equally spaced sub-intervals and defining all the possible combinations of values. Hence, the RAM usage of the implementation in Grana et al. (2021) increases exponentially with the number of variables of the joint distribution. Instead, the DMS implementation is based on a set of N_s training data points stored in a matrix with dimensions $N_s \times (p + q)$. Hence, the DMS implementation significantly reduces the RAM usage compared to rock-physics inversion methods that require the evaluation of the full non-parametric joint distribution.

In this application, we use $p = 3$ and $q = 3$ variables and $n_p = 350$ data points, whereas for the traditional implementation we assume that each variable domain is discretized in an interval with $L = 25$ points. The values of n_p for DMS and L for the traditional implementation were chosen to achieve similar processing times for the two methods and focus the comparison in terms of RAM usage. Assuming double precision, the RAM usage of the two methods is shown in Table 3.

The traditional implementation can be improved in terms of RAM consumption by using a numerical sparse matrix

	Traditional approach	DMS approach
RAM usage (MB)	1,819.0	3.1

Table 3

RAM memory usage of traditional and DMS approaches.

325 to store the joint distribution, but this implementation still highly depends on the number of variables. Instead, the
 326 proposed approach allows for the application of the methodology to high-dimensional problems with limited RAM
 327 usage.

328 3.2. Time-lapse synthetic example

329 This example is based on the benchmark model UNISIM-I (Avansi and Schiozer, 2015). The dataset represents
 330 a 3D reservoir model with data available at two different times, namely the base and monitor times in year 2013 and
 331 2024 respectively. The reservoir properties are defined in a 3D geocellular model based on public data from Namorado
 332 Field, Brazil. In this work, we use the properties of the 20th layer of the reservoir model. The model includes 11 water
 333 injection wells and 10 production wells. Fig. 3 shows the petrophysical models of porosity, base water saturation
 334 (s_{w1}), and monitor water saturation (s_{w2}). Porosity is assumed to be variable in space but constant in time. Pressure
 335 and mineralogy are assumed to be known and constant. We define three facies, namely shale, mid-porosity sand, and
 336 high-porosity sand. The petrophysical models are used to compute the synthetic time-lapse dataset. The rock physics
 337 model is based on the soft sand model with Gassmann's equation (Mavko et al., 2009; Grana et al., 2021). The rock
 338 physics model computes P- and S-wave velocity and density, from which P-impedance and V_P/V_S velocity ratio are
 339 calculated. The rock and fluid parameters are shown in Table 4. Reservoir conditions are assumed to be known with
 340 temperature 80° C and effective pressure 60 MPa. The synthetic time-lapse dataset, $m = \left(I_{P1}, I_{P2}, \left(\frac{V_P}{V_S} \right)_1, \left(\frac{V_P}{V_S} \right)_2 \right)$,
 341 includes two elastic properties, specifically P-impedance and V_P/V_S velocity ratio, at the base and monitor surveys.

342 The statistical model of the error of the elastic properties is a multivariate Gaussian distribution with zero mean
 343 and covariance Σ_m . The covariance matrix Σ_m is defined as the Kronecker product of a covariance matrix of the elastic
 344 properties and a spatially dependent correlation matrix computed from a spatial correlation model (Buland and Omre,
 345 2003; Grana et al., 2021). In this application, the spatial model is an exponential correlation function with isotropic
 346 correlation range of 15 grid cells. The standard deviations are 75 m/s for P-wave velocity, 37.5 m/s for S-wave velocity,
 347 and 0.075 g/cm³ for density. Fig. 4 shows the calculated elastic properties for the base and monitor times. The models
 348 of elastic properties at the base and monitor times are then used as input for the rock-physics inversion.

349 We assume no prior correlation among the petrophysical properties in the prior components $p(\mathbf{r}|\pi)$ of Equation 5.
 350 For porosity, we assume a facies-dependent truncated Gaussian mixture with parameters fitted to match the empirical
 351 distribution from well logs. For water saturation, we assume uniform distributions in the mid- and high-porosity sand
 352 facies and a truncated Gaussian distribution in shale. The parameter values of each distribution are listed in Table

K_m (GPa)	G_m (GPa)	ρ_m (g/cm ³)	K_w (GPa)	ρ_w (g/cm ³)	K_o (GPa)	ρ_o (g/cm ³)	ϕ_c	c_n
37	44	2.65	3.14	1.06	0.53	0.52	0.4	9

Table 4

Rock-physics parameters: K_m and G_m are the mineral elastic moduli, ρ_m is the mineral density, K_w is the brine bulk modulus brine, ρ_w is the brine density, K_o if the oil bulk modulus, ρ_o is the oil density, ϕ_c is the critical porosity, and c_n is the coordination number.

	shale	mid-porosity sand	high-porosity sand
porosity	$\mathcal{N}(0.02, 0.005) [0, 0.4]$	$\mathcal{N}(0.1, 0.05) [0, 0.4]$	$\mathcal{N}(0.25, 0.05) [0, 0.4]$
water saturation s_{w1}	$\mathcal{N}(0.9, 0.02) [0, 1]$	$U(0, 1)$	$U(0, 1)$
water saturation s_{w2}	$\mathcal{N}(0.9, 0.02) [0, 1]$	$U(0, 1)$	$U(0, 1)$

Table 5

Parameters of the prior Gaussian mixture model for porosity, base water saturation, and monitor water saturation. $\mathcal{N}(\mu, \sigma) [\min, \max]$ denotes a truncated Gaussian distribution with mean μ and standard deviation σ , and truncated minimum and maximum values, min and max.

353 5. The crossplot and the marginal histograms of porosity and water saturation are shown in Fig. 5 together with the
 354 contours of the distributions of the prior components and their marginal distributions.

355 Then, we perform a Monte Carlo sampling to generate samples from the joint distribution $p(\mathbf{m}, \mathbf{r})$. We draw 50000
 356 samples of each petrophysical property $\{\mathbf{r}^i\}$ for each facies, and then sample P- and S-wave velocity and density at the
 357 base and monitor times, from a Gaussian distribution with mean $f(\mathbf{r}^i)$ obtained from the rock-physics model. From the
 358 multiple samples $\{\mathbf{m}^i\}$, we then compute acoustic impedance and V_P/V_S velocity ratio at the base and monitor times.
 359 The joint distribution computed from the prior sampling $\{\mathbf{r}^i, \mathbf{m}^i\}$ is shown in Fig. 6, where we show the bivariate
 360 marginal histograms of all pairs of properties and the univariate marginal histograms, computed from the 7-variate
 361 joint distribution. Fig. 6 shows the non-linear and heteroscedastic relations among the variables.

362 We then apply the inversion methodology using the joint distribution obtained by Monte Carlo sampling $\{\mathbf{r}^i, \mathbf{m}^i\}_{i=1, \dots, N_s}$.
 363 First, we compute the spatially uncorrelated median models of the petrophysical properties without hard data condi-
 364 tioning (Fig. 7a) and with data conditioning (Fig. 7b). For the inversion with hard data conditioning, the well data
 365 are transformed into the Gaussian distributed space and a simple kriging with zero mean and unit variance is used to
 366 interpolate the values in grid. As a result, the inverted median models in Fig. 7b honor the well log data.

367 Then, we simulate multiple spatially correlated non-parametric realizations conditioned on the well data, dis-
 368 tributed according to the joint distribution. Based on the well data transformed into the Gaussian distributed space, we
 369 draw multiple Gaussian realizations conditioned to the transformed well data. Fig. 8 shows two different geostatistical
 370 realizations. The models reproduce spatial correlated features and honor well log data. The pointwise median values
 371 based on multiples realizations are shown in Fig. 9a and match the results in Fig. 7b. Fig. 9b shows the pointwise
 372 standard deviation of multiple realizations. The low values of standard deviation around the well locations prove the
 373 effectiveness of the data conditioning. The inverted water saturation models exhibit greater variability compared to

	Unconditional median (Fig. 7a)	Conditional median (Fig. 7b)	Median of simulations (Fig. 9a)
RMSE	0.4957	0.4019	0.4037

Table 6

Root mean square error between the median models and the reference petrophysical models.

374 porosity, due to the higher prior variance, bimodality of the distribution, and lower sensitivity of saturation to the
 375 elastic parameters.

376 To quantitatively assess the results, we compute the root mean square error (RMSE) of the median models (Table
 377 6). The results show lower errors for the conditional median models in Figs. 7b and 9a, than the unconditional median
 378 models in Fig. 7a. Finally, to evaluate the ability of the method to reproduce the non-parametric PDF, we show the
 379 bivariate and univariate marginal histograms of the the 7-variate distribution in Fig. 10. The comparison between Fig.
 380 10 and Fig. 6 demonstrates that the joint distribution of the geostatistical realizations present the same characteristics
 381 of the joint distribution of the Monte Carlo samples, with non-linear and heteroscedastic relations among the variables.

382 4. Conclusions

383 We present a new algorithm for non-linear and non-parametric geostatistical rock-physics inversion of elastic prop-
 384 erties to predict the petrophysical properties of interest. The methodology combines statistical rock-physics modeling,
 385 stepwise conditional transformation, and direct multivariate simulation for the generation of conditional realizations
 386 of the petrophysical properties. The proposed algorithm efficiently estimates the petrophysical properties while main-
 387 taining spatial correlations and honoring hard data conditioning. The input of the algorithm is a joint multivariate dis-
 388 tribution of both elastic and petrophysical properties, which is represented by a training dataset. The training dataset
 389 may consist of well logs if they are representative of all possible reservoir conditions, or it may be a set of Monte
 390 Carlo samples generated with statistical rock-physics modeling. When using Monte Carlo, facies-dependent mixture
 391 prior models can be assumed, where the mixture components should be defined according to well data and geological
 392 knowledge of the rocks. The joint distribution of petrophysical and elastic properties is non-parametric due to the non-
 393 linearity of the rock-physics model. The joint distribution is then used to conditionally sample posterior realizations
 394 of the petrophysical properties conditioned to the input elastic variables. In comparison to a traditional method for
 395 rock-physics inversion, the algorithm demonstrates significant improvements in terms of RAM usage, which makes
 396 methodology suitable for high-dimensional inverse problems. The method is validated in a real case study using well
 397 logs, where we adopted a 6-variate joint distribution for the estimation of petrophysical properties. Then, the method
 398 is applied to a time-lapse study using a 7-variate distribution for the estimation of porosity and saturation changes. In
 399 the second application, we simulate the median model conditioned to elastic properties only, the median model con-
 400 ditioned to seismic properties and direct measurements, and multiple geostatistical realizations conditioned to seismic

401 properties and direct measurements. The multiple realizations provide a comprehensive set of models for uncertainty
402 quantification. The results show that the non-linear and heteroscedastic relationships among variables observed in
403 the joint distributions are preserved, leading to accurate model predictions. Furthermore, we demonstrate that hard
404 data conditioning significantly enhances results, highlighting a key advantage of the proposed method over traditional
405 approaches, such as point-by-point inversion, that do not account for lack spatial conditioning, .

406 **5. Acknowledgments**

407 Authors acknowledge Petrobras/CENPES, LTrace and the School of Energy Resources of the University of Wyoming
408 for the support.

409 **Code availability section**

410 GeoStatRPIInv - Non-linear and Non-parametric GeoStatistical rock-physics inversion of elastic properties

411 Contact: leandro@ltrace.com.br and +55 991 445 020

412 No hardware requirements.

413 Program language: Matlab

414 Software required: Matlab 2021

415 Program size: 50MB

416 The source codes are available for downloading at the link:

417 <https://github.com/leandrorfgr/GeoStatRockPhysics>418 **References**

- 419 Abulkhair, S., Dowd, P., Xu, C., 2023. Geostatistics in the presence of multivariate complexities: Comparison of multi-gaussian transforms.
420 Mathematical Geosciences 55. doi:10.1007/s11004-023-10056-y.
- 421 Aleardi, M., 2018. Estimating petrophysical reservoir properties through extended elastic impedance inversion: applications to off-shore and
422 on-shore reflection seismic data. Journal of Geophysics and Engineering 15, 2079–2090. URL: <https://doi.org/10.1088/1742-2140/aac54b>, doi:10.1088/1742-2140/aac54b.
- 423 Aleardi, M., Ciabarri, F., Mazzotti, A., 2017. Probabilistic estimation of reservoir properties by means of wide-angle ava inversion and a petro-
424 physical reformulation of the zoeppritz equations. Journal of Applied Geophysics 147, 28–41. URL: <https://www.sciencedirect.com/science/article/pii/S0926985117301192>, doi:<https://doi.org/10.1016/j.jappgeo.2017.10.002>.
- 425 Avalos, S., Ortiz, J., 2023a. Multivariate geostatistical simulation and deep q-learning to optimize mining decisions. Mathematical Geosciences
426 55. doi:10.1007/s11004-023-10049-x.
- 427 Avalos, S., Ortiz, J.M., 2023b. Spatial multivariate morphing transformation. Mathematical Geosciences 55, 735–771.
- 428 Avansi, G., Schiozer, D., 2015. Unisim-i: synthetic model for reservoir development and management applications. Int. J. Model. Simul. Pet. Ind.
429 9, 21–30.
- 430 Avseth, P., Mukerji, T., Mavko, G., 2005. Quantitative seismic interpretation. Cambridge University Press.
- 431 Bachrach, R., 2006. Joint estimation of porosity and saturation using stochastic rock-physics modeling. Geophysics 71, O53–O63. URL: <https://doi.org/10.1190/1.2235991>, doi:10.1190/1.2235991, arXiv:<https://doi.org/10.1190/1.2235991>.
- 432 Barnett, R.M., Manchuk, J.G., Deutsch, C.V., 2014. Projection pursuit multivariate transform. Mathematical Geosciences 46, 337–359. doi:10.
433 1007/s11004-013-9497-7.
- 434 Berg, B.A., Harris, R.C., 2008. From data to probability densities without histograms. Computer Physics Communications 179, 443–448. URL:
435 <https://doi.org/10.1016/j.cpc.2008.03.010>, doi:10.1016/j.cpc.2008.03.010.
- 436 Bertsekas, D., Tsitsiklis, J., 2008. Introduction to Probability. Athena Scientific optimization and computation series, Athena Scientific.
- 437 Bosch, M., Carvajal, C., Rodrigues, J., Torres, A., Aldana, M., Sierra, J., 2009. Petrophysical seismic inversion conditioned to well-log data:
438 Methods and application to a gas reservoir. GEOPHYSICS 74, O1–O15. URL: <https://doi.org/10.1190/1.3043796>, doi:10.1190/1.
439 3043796, arXiv:<https://doi.org/10.1190/1.3043796>.

- 443 Bosch, M., Mukerji, T., Gonzalez, E., 2010. Seismic inversion for reservoir properties combining statistical rock physics and geostatistics: A review.
 444 Geophysics 75, 75A165–75A176.
- 445 Buland, A., Omre, H., 2003. Bayesian linearized AVO inversion. Geophysics 68, 185–198. doi:10.1190/1.1543206.
- 446 Caers, J., 2011. Engineering the Earth: Making Decisions Under Uncertainty. John Wiley & Sons, Ltd. chapter 4. pp. 55–76. URL: <https://onlinelibrary.wiley.com/doi/abs/10.1002/9781119995920.ch4>, doi:<https://doi.org/10.1002/9781119995920.ch4>.
- 447 de Figueiredo, L.P., Schmitz, T., Lunelli, R., Roisenberg, M., Santana de Freitas, D., Grana, D., 2021. Direct multivariate simulation - a step-
 448 wise conditional transformation for multivariate geostatistical simulation. Computers & Geosciences 147, 104659. URL: <https://www.sciencedirect.com/science/article/pii/S0098300420306336>, doi:<https://doi.org/10.1016/j.cageo.2020.104659>.
- 450 Doyen, P., 2007. Seismic reservoir characterization: an earth modelling perspective. Education tour series, EAGE publications.
- 451 de Figueiredo, L.P., Grana, D., Bordignon, F.L., Santos, M., Roisenberg, M., Rodrigues, B.B., 2018. Joint bayesian inversion based on rock-physics
 452 prior modeling for the estimation of spatially correlated reservoir properties. GEOPHYSICS 83, M49–M61. URL: <https://doi.org/10.1190/geo2017-0463.1>, doi:10.1190/geo2017-0463.1, arXiv:<https://doi.org/10.1190/geo2017-0463.1>.
- 453 de Figueiredo, L.P., Grana, D., Roisenberg, M., Rodrigues, B.B., 2019. Gaussian mixture markov chain monte carlo method for linear seis-
 454 mic inversion. GEOPHYSICS 84, R463–R476. URL: <https://doi.org/10.1190/geo2018-0529.1>, doi:10.1190/geo2018-0529.1,
 455 arXiv:<https://doi.org/10.1190/geo2018-0529.1>.
- 456 Fjeldstad, T., Grana, D., 2017. Joint probabilistic petrophysics-seismic inversion based on Gaussian mixture and markov chain prior models.
 457 Geophysics , 1–46doi:10.1190/geo2017-0239.1.
- 458 Gómez-Hernández, J.J., Journel, A.G., 1993. Joint sequential simulation of MultiGaussian fields, in: Quantitative Geology and Geostatistics.
 459 Springer Netherlands, pp. 85–94. URL: https://doi.org/10.1007/978-94-011-1739-5_8, doi:10.1007/978-94-011-1739-5_8.
- 460 Grana, D., 2016. Bayesian linearized rock-physics inversion. Geophysics 81, D625–D641.
- 461 Grana, D., Azevedo, L., De Figueiredo, L., Connolly, P., Mukerji, T., 2022a. Probabilistic inversion of seismic data for reservoir petrophysical
 462 characterization: Review and examples. Geophysics 87, M199–M216.
- 463 Grana, D., Della Rossa, E., 2010. Probabilistic petrophysical-properties estimation integrating statistical rock physics with seismic inversion.
 464 Geophysics 75, O21–O37. doi:10.1190/1.3386676.
- 465 Grana, D., Liu, M., de Figueiredo, L., 2024. Geospin: A matlab library for geostatistical petrophysical inversion. GEOPHYSICS 0, 1–57. URL:
 466 <https://doi.org/10.1190/geo2023-0467.1>, doi:10.1190/geo2023-0467.1.
- 467 Grana, D., Mukerji, T., Doyen, P., 2021. Seismic reservoir modeling: Theory, examples, and algorithms. John Wiley & Sons.
- 468 Grana, D., Russell, B., Mukerji, T., 2022b. Petrophysical inversion based on f-s-r amplitude-variation-with-offset linearization and canonical corre-
 469 lation analysis. GEOPHYSICS 87, M247–M258. URL: <https://doi.org/10.1190/geo2021-0747.1>, doi:10.1190/geo2021-0747.1,
 470 arXiv:<https://doi.org/10.1190/geo2021-0747.1>.
- 471 Guo, Q., Ba, J., Luo, C., 2022. Nonlinear petrophysical amplitude variation with offset inversion with spatially variable pore as-
 472 pect ratio. GEOPHYSICS 87, M111–M125. URL: <https://doi.org/10.1190/geo2021-0583.1>, doi:10.1190/geo2021-0583.1,
 473 arXiv:<https://doi.org/10.1190/geo2021-0583.1>.
- 474 Guo, Q., Ba, J., Luo, C., 2023. Seismic rock-physics linearized inversion for reservoir-property and pore-type parameters with application to
 475 carbonate reservoirs. Geoenergy Science and Engineering 224, 211640. URL: <https://www.sciencedirect.com/science/article/pii/S2949891023002270>, doi:<https://doi.org/10.1016/j.geoen.2023.211640>.
- 476 Horta, A., Soares, A., 2010. Direct sequential co-simulation with joint probability distributions. Mathematical Geosciences 42, 269–292. URL:
 477 <https://doi.org/10.1007/s11004-010-9265-x>, doi:10.1007/s11004-010-9265-x.

Geostatistical rock-physics inversion

- 481 Leonardo Azevedo, A.S., 2017. Geostatistical Methods for Reservoir Geophysics. Springer International Publishing. doi:10.1007/
482 978-3-319-53201-1.
- 483 Leuangthong, O., Deutsch, C., 2003. Stepwise conditional transformation for simulation of multiple variables. Mathematical Geosciences 35,
484 155–173. doi:doi.org/10.1023/A:1023235505120.
- 485 Liu, M., Grana, D., 2018. Stochastic nonlinear inversion of seismic data for the estimation of petroelastic properties using the ensemble smoother
486 and data reparameterization. GEOPHYSICS 83, M25–M39. doi:10.1190/geo2017-0713.1.
- 487 Mavko, G., Mukerji, T., Dvorkin, J., 2009. The Rock Physics Handbook. Second ed., Cambridge University Press. Cambridge Books Online.
- 488 Sen, M.K., 2006. Seismic Inversion. Society of Petroleum Engineers, Richardson, TX, USA.
- 489 Shahraeeni, M.S., Curtis, A., 2011. Fast probabilistic nonlinear petrophysical inversion. GEOPHYSICS 76, E45–E58. URL: <https://doi.org/10.1190/1.3540628>, doi:10.1190/1.3540628, arXiv:<https://doi.org/10.1190/1.3540628>.
- 490 Soares, A., 2001. Direct sequential simulation and cosimulation. Mathematical Geology 33, 911–926.
- 491 Tarantola, A., 2005. Inverse Problem Theory and Methods for Model Parameter Estimation. Society for Industrial and Applied Mathematics.
- 492 Teillet, T., Fournier, F., Zhao, L., Borgomano, J., Hong, F., 2021. Geophysical pore type inversion in carbonate reservoir: Integration of
493 cores, well logs, and seismic data (yadana field, offshore myanmar). GEOPHYSICS 86, B149–B164. URL: <https://doi.org/10.1190/geo2020-0486.1>, doi:10.1190/geo2020-0486.1.
- 494 van der Waerden, B., Thompson, V., Sherman, E., 1969. Mathematical Statistics. Die Grundlehren der mathematischen Wissenschaften in Einzel-
495 darstellungen, Springer. URL: <https://books.google.com.br/books?id=Cd8gQgAACAAJ>.

498 **List of Figures**

499 1	Schematic representation of the DMS-based geostatistical inversion.	20
500 2	Well log dataset including facies, P- and S-wave velocities, density, porosity, clay volume, and water saturation, and inversion results. The reference well logs are shown in black, the inversion median results in red, and 20 geostatistical realizations in gray.	21
501 3	Reference petrophysical properties. From left to right: porosity, water saturation of the base survey, and water saturation of the monitor survey. <i>I</i> and <i>J</i> indicate the coordinates of the Cartesian grid with the corresponding grid cell numbers.	22
502 4	Elastic properties: P-impedance on the left and V_P/V_S ratio on the right.	23
503 5	Prior distribution of water saturation and porosity and well log data: a) marginal histogram of water saturation and prior components of the marginal distribution; b) crossplot of well log data of water saturation and porosity and contours of the prior component distributions; and c) marginal histogram of water saturation and prior components of the marginal distribution (shale in gray, mid-porosity sand in yellow, and high-porosity sand in green).	24
504 6	Bivariate and univariate marginal histograms of Monte Carlo samples obtained from the 7-variate non-parametric joint distribution according to the prior distribution of the petrophysical properties and the non-linear rock-physics model.	25
505 7	Inverted median models of petrophysical properties without hard data conditioning (a) and with hard data conditioning (b).	26
506 8	Two geostatistical realizations of petrophysical properties conditioned to the well data (hard data) and elastics properties.	27
507 9	Pointwise median (a) and standard deviation (b) of geostatistical realizations of petrophysical properties conditioned to the well data (hard data) and elastics properties.	28
508 10	Bivariate and univariate marginal histograms of geostatistical realizations obtained from the 7-variate non-parametric joint distribution according to the prior distribution of the petrophysical properties and the non-linear rock-physics model.	29
509		
510		
511		
512		
513		
514		
515		
516		
517		
518		
519		
520		
521		
522		
523		

Geostatistical rock-physics inversion

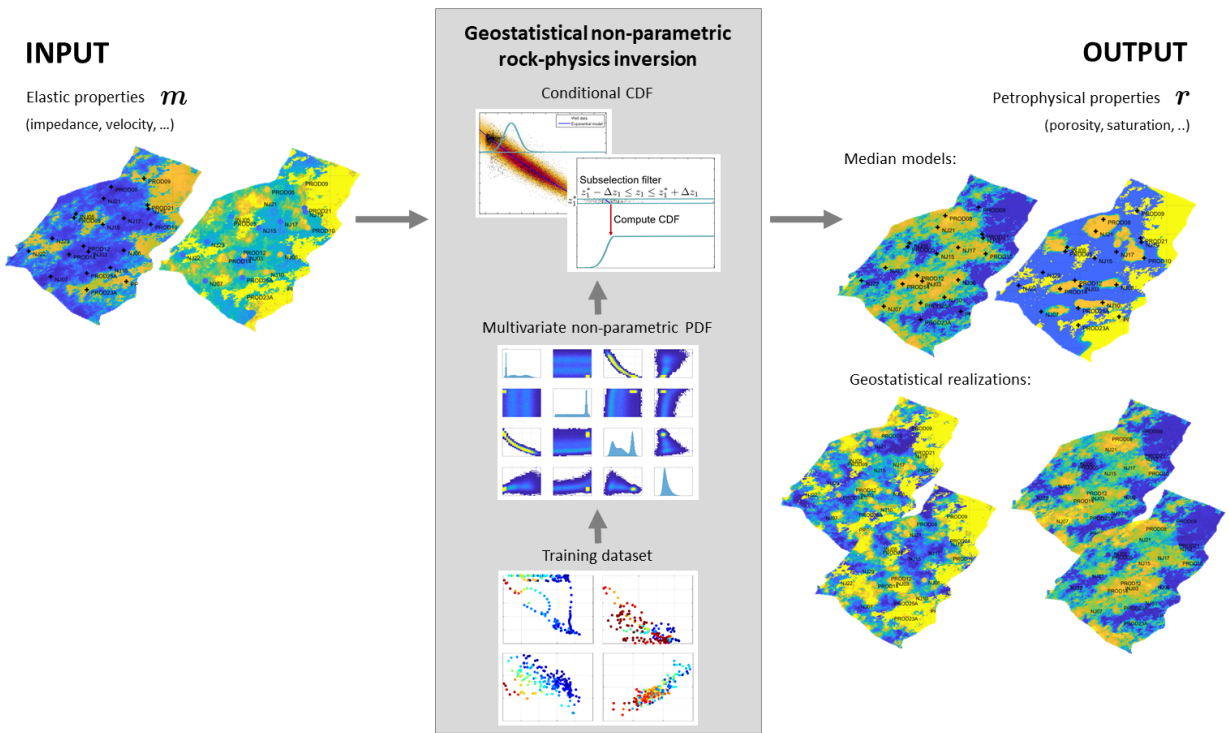


Figure 1: Schematic representation of the DMS-based geostatistical inversion.

Geostatistical rock-physics inversion

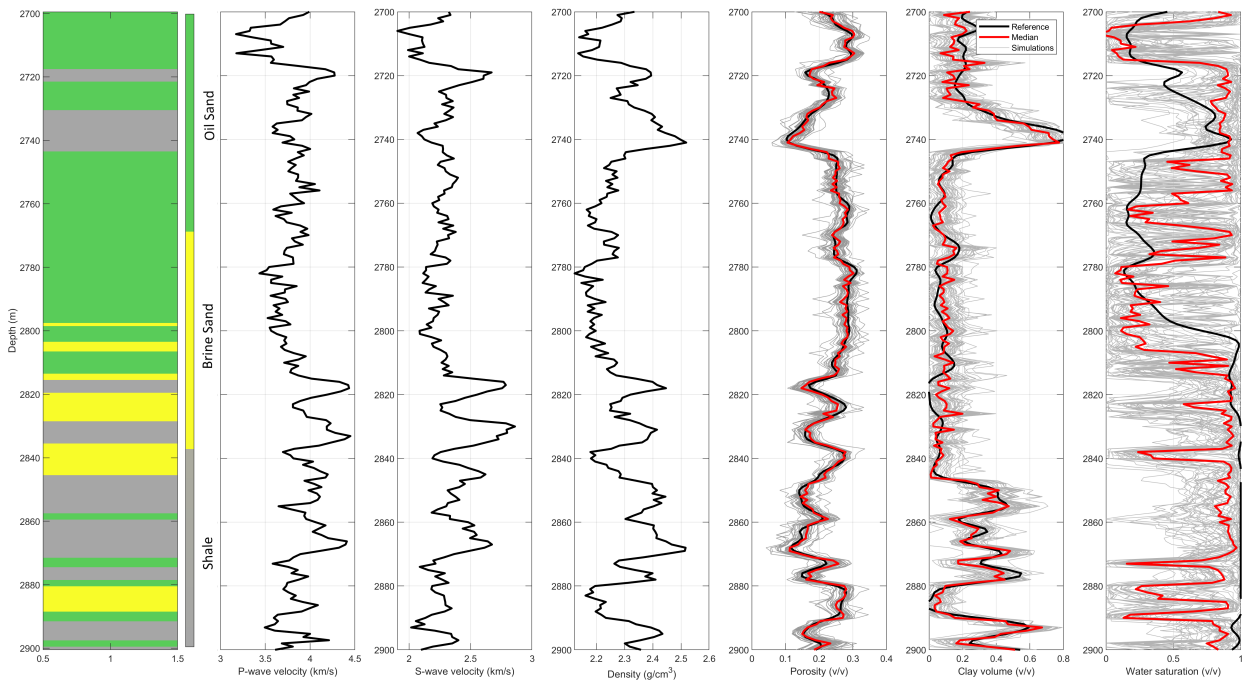


Figure 2: Well log dataset including facies, P- and S-wave velocities, density, porosity, clay volume, and water saturation, and inversion results. The reference well logs are shown in black, the inversion median results in red, and 20 geostatistical realizations in gray.

Geostatistical rock-physics inversion

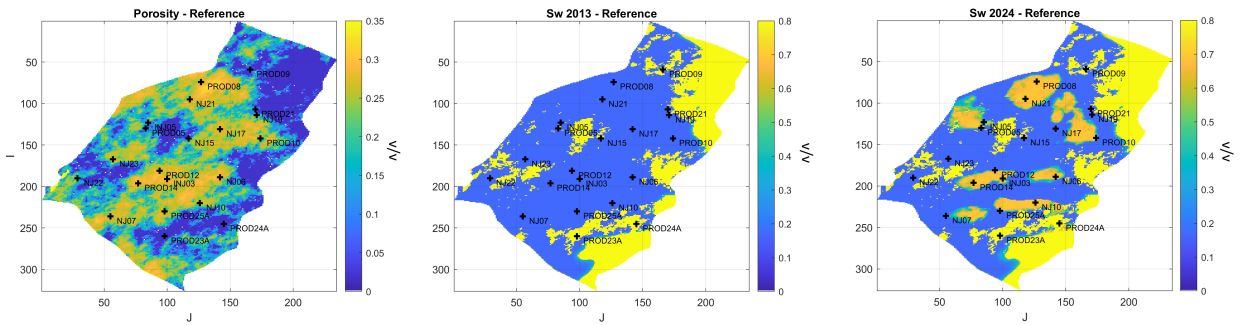


Figure 3: Reference petrophysical properties. From left to right: porosity, water saturation of the base survey, and water saturation of the monitor survey. I and J indicate the coordinates of the Cartesian grid with the corresponding grid cell numbers.

Geostatistical rock-physics inversion

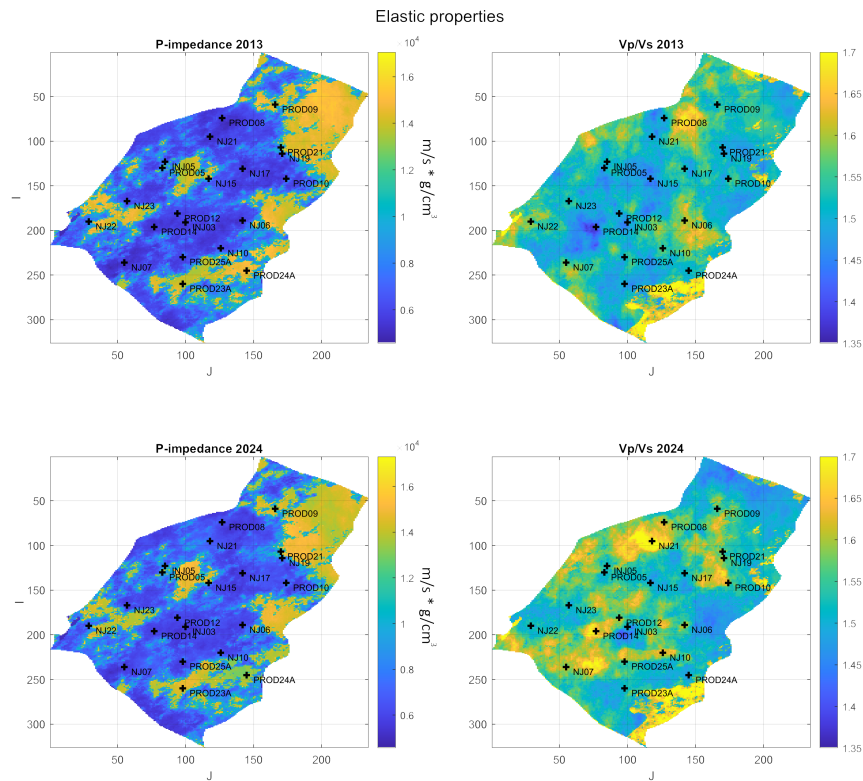


Figure 4: Elastic properties: P-impedance on the left and V_p/V_s ratio on the right.

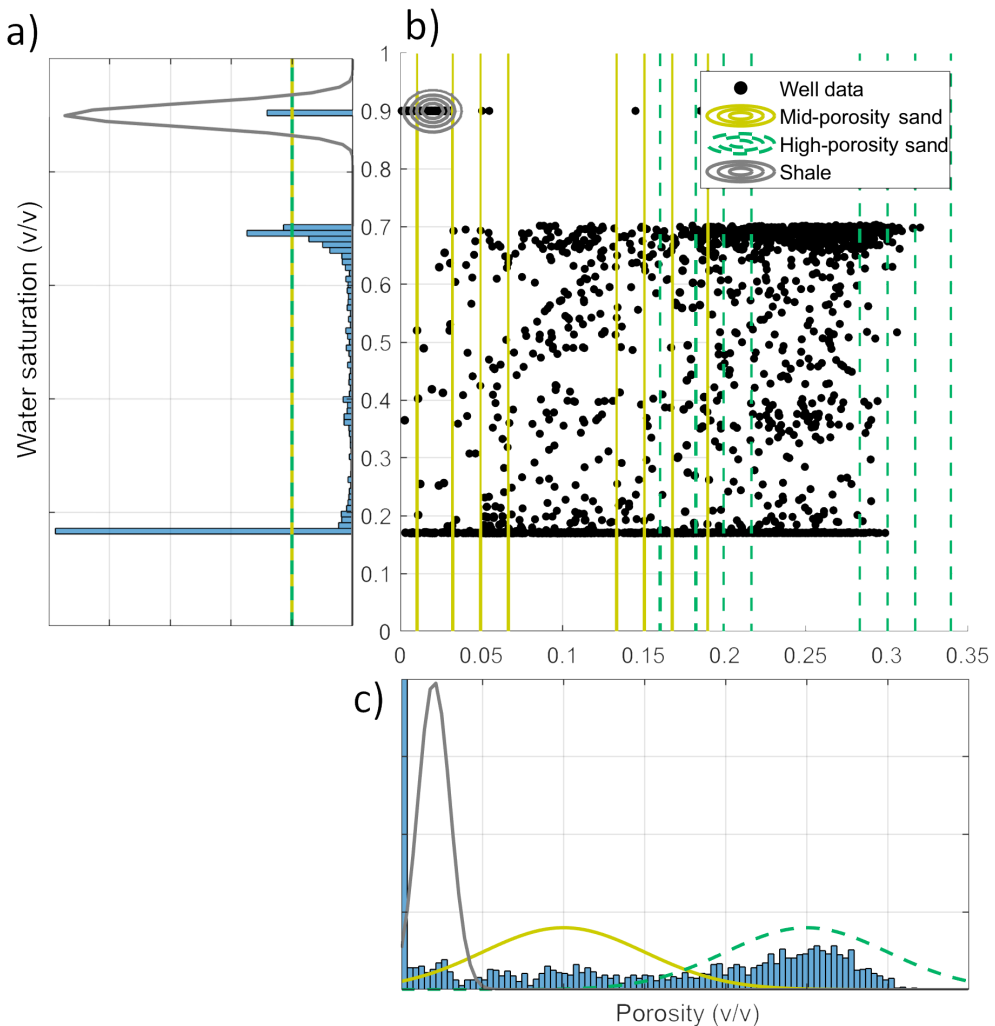


Figure 5: Prior distribution of water saturation and porosity and well log data: a) marginal histogram of water saturation and prior components of the marginal distribution; b) crossplot of well log data of water saturation and porosity and contours of the prior component distributions; and c) marginal histogram of water saturation and prior components of the marginal distribution (shale in gray, mid-porosity sand in yellow, and high-porosity sand in green).

Geostatistical rock-physics inversion

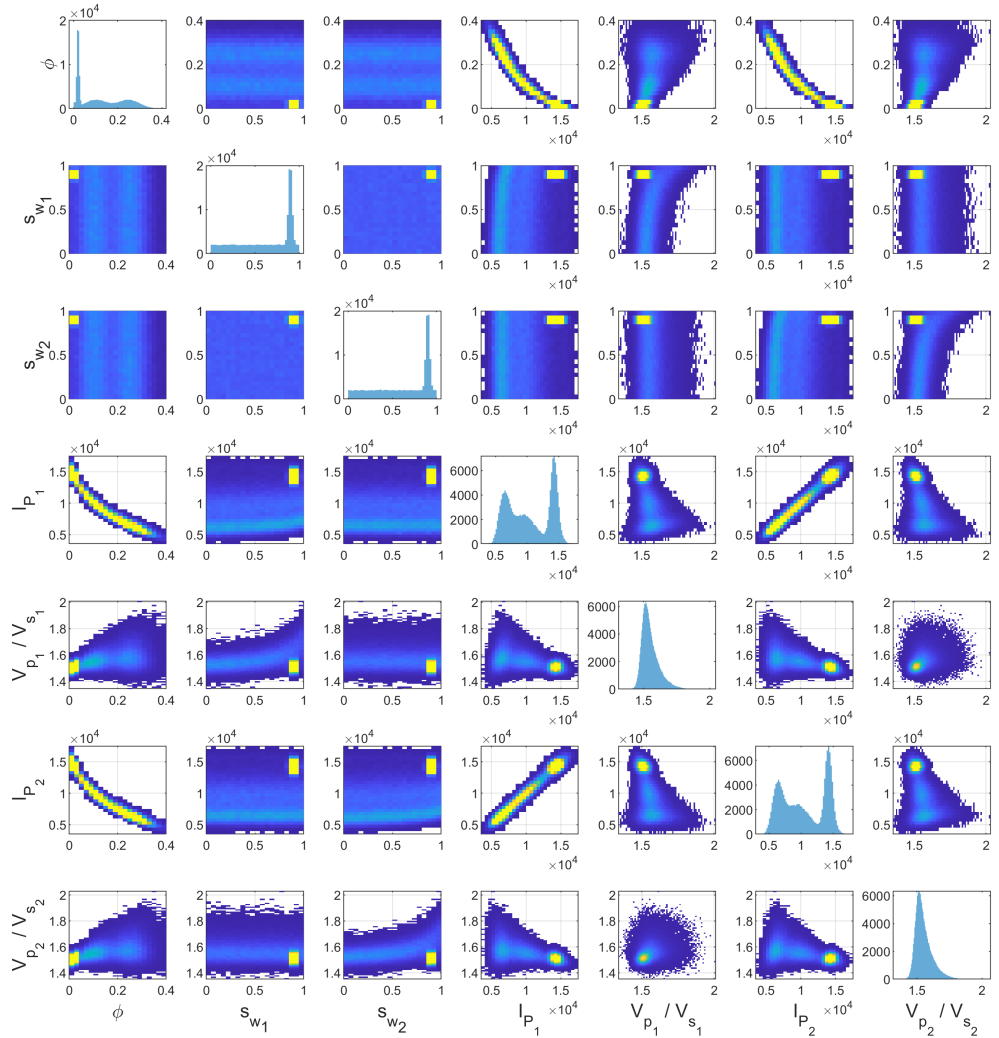


Figure 6: Bivariate and univariate marginal histograms of Monte Carlo samples obtained from the 7-variate non-parametric joint distribution according to the prior distribution of the petrophysical properties and the non-linear rock-physics model.

Geostatistical rock-physics inversion

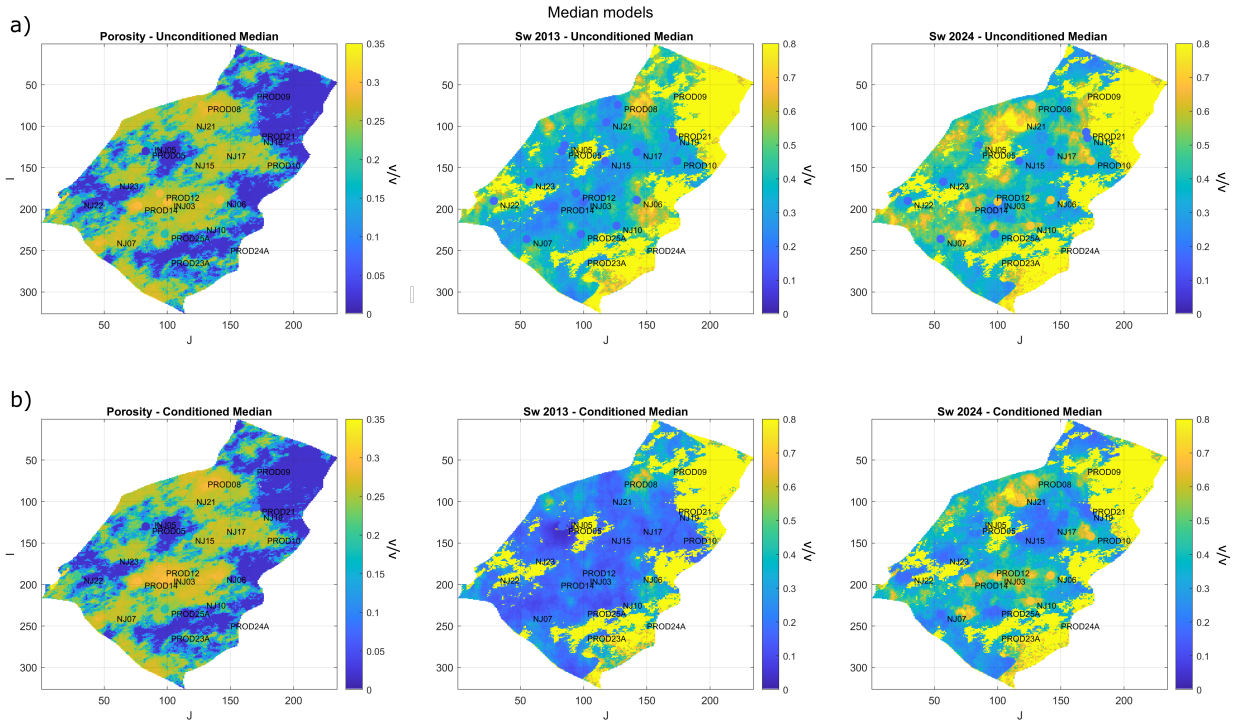


Figure 7: Inverted median models of petrophysical properties without hard data conditioning (a) and with hard data conditioning (b).

Geostatistical rock-physics inversion

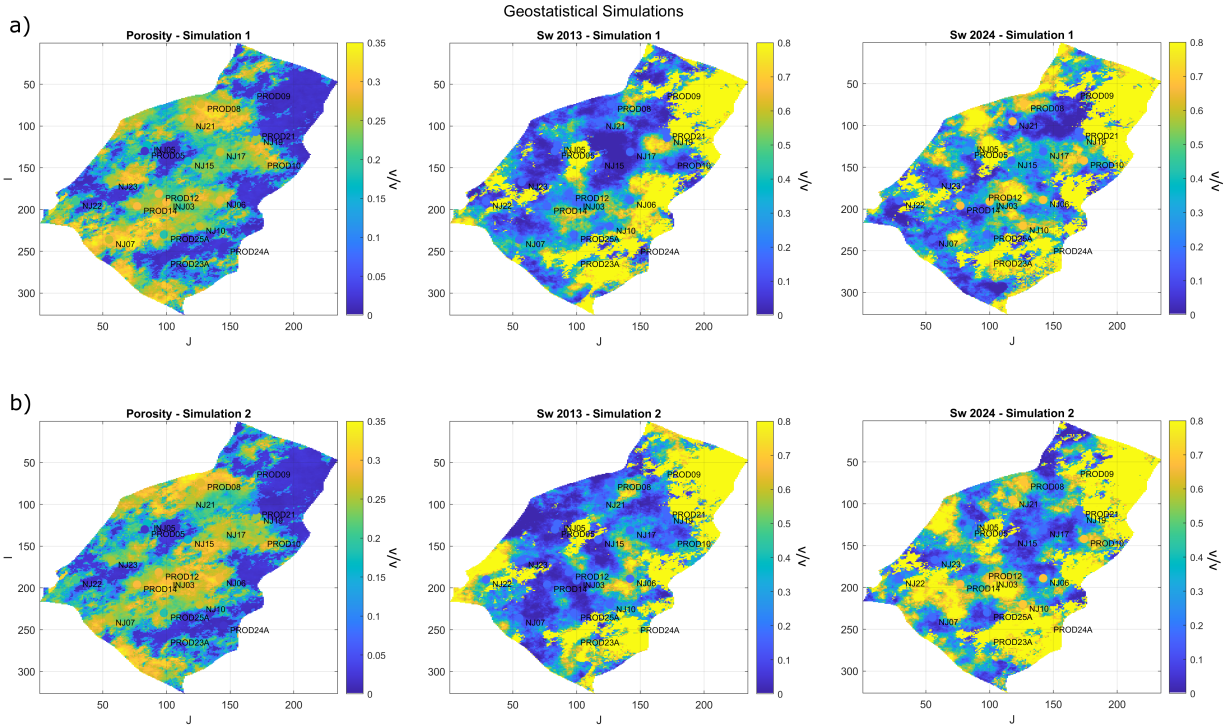


Figure 8: Two geostatistical realizations of petrophysical properties conditioned to the well data (hard data) and elastics properties.

Geostatistical rock-physics inversion

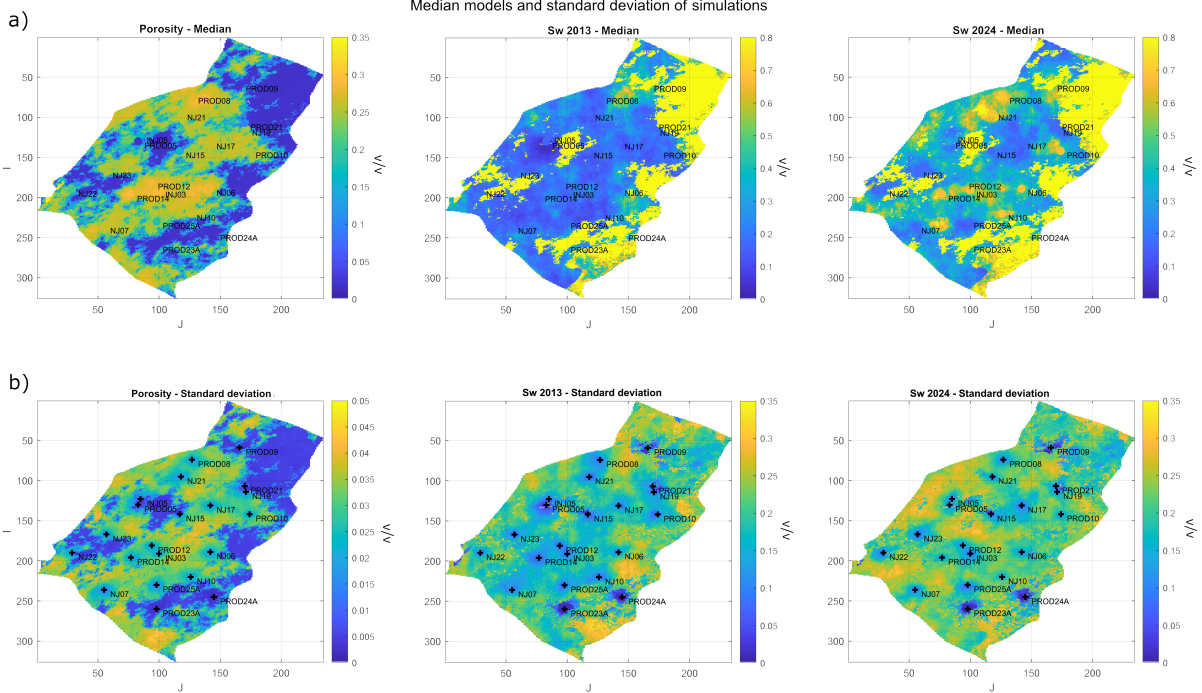


Figure 9: Pointwise median (a) and standard deviation (b) of geostatistical realizations of petrophysical properties conditioned to the well data (hard data) and elastics properties.

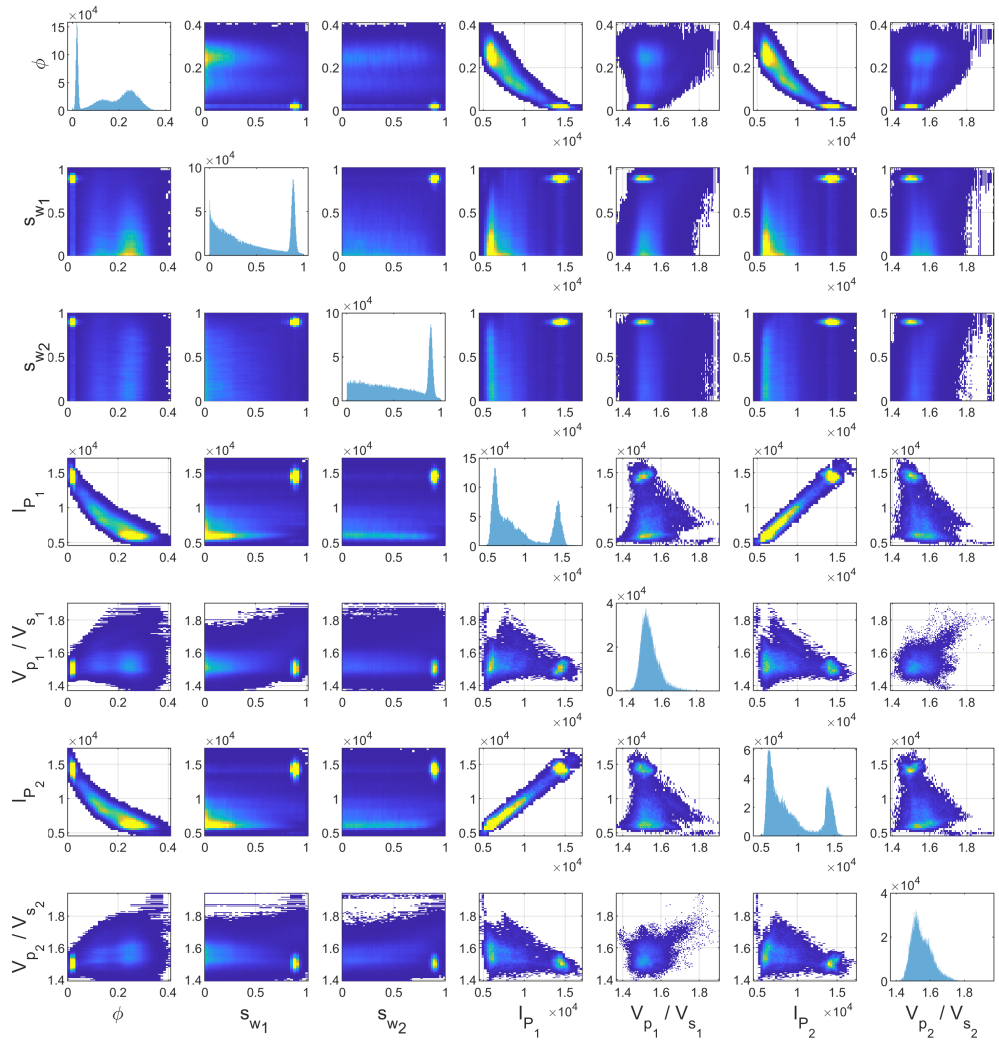


Figure 10: Bivariate and univariate marginal histograms of geostatistical realizations obtained from the 7-variate non-parametric joint distribution according to the prior distribution of the petrophysical properties and the non-linear rock-physics model.